Simulating the Measurement of the Electron Beam Emittance at AWAKE

Patrick Chin

Contents

1 Introduction **4**

2 Proton Driven Plasma Wakefield Acceleration **4**

3 AWAKE **4**
3.1 Self-modulation instability 4
3.2 Uniform-density plasma cell 4
3.3 Injection of the witness beam 4
3.4 AWAKE 5

4 Project outline **5**

5 Single Particle Dynamics **6**

6 Emittance **6**

7 The Simulation **7**
7.1 The Electron Beam 7
7.1.1 BDSIM calibration 7
7.1.2 Deriving the Beam Size Function . . 7
7.2 Backgrounds 7
7.3 Error Calculations 7
7.4 Binning errors 8

8 Results **9**
8.1 Energy Spread 9
8.2 Input Emittance 9
8.3 Background Photons 9

9 Conclusion **10**

1. Introduction

Advancements in quantum and particle physics are primarily driven by experimental observations which can verify or refute previous hypotheses, or can provide data from which new hypotheses can be drawn. Particle colliders are a main source of observational data at the quantum scale, and can create millions of collision events every second.

Proton–proton beam energies at the Large Hadron Collider (LHC) have recently reached energies of 13 TeV [1], whereas lepton–lepton colliders have yet to reach the TeV energy scale. The largest of which, the Large Electron-Proton Collider (LEP), was closed down to make way for the LHC in 2000 after having reached a maximum energy of 209 GeV [2].

- reasons why lepton collisions are cleaner than protons
- drawbacks of circular accelerator synchrotron radiation at LEP [3]
- ICL and CLIC proposed linear RF accelerators ten times larger than SLAC

The CLIC and ICL are promising proposals for lepton–lepton colliders to reach the TeV scale, however

continuing to increase the energy of colliding beams allows for an increasing number of interactions to be observed.

2. Proton Driven Plasma Wakefield Acceleration

Current radio-frequency (RF) accelerator technology is limited to an electromagnetic gradient of about $100\,\mathrm{MeV\,m^{-1}}$ due to RF beakdown. The ability of plasma to sustain very large

The concept of accelerating particles in plasma was promising as plasma is able to sustain large electric fields. The idea being that energy can be transferred to a group of charged particles by injecting them into the plasma wakefield that follows a high energy laser pulse or proton bunch, using the plasma as an energy transfer medium. The witness bunch is then accelerated by the high electromagnetic gradient.

3. AWAKE

3.1. Self-modulation instability

The first challenge in the development of this accelerator was getting the length of the proton driver bunch small enough so that resonance occurs with the electrons in the plasma. Typical proton bunches, i.e. those produced by the CERN Super Proton Synchrotron (SPS), have lengths of $\sim 10\,\mathrm{cm}$ which cannot directly create strong plasma waves at the required wavelength in the mm scale as the Fourier component of the proton beam at the plasma frequency is negligible. Simulations [4] on the compression of these bunches show that reducing the longitudinal phase volume blows up the transverse phase volume. An alternative method would be to split up the proton bunch into a number of micro-bunches to be simultaneously decelerated.

An instability between the beam and the plasma arises from the mutual amplification of the rippling of the beam radius and the plasma wave. This instability tends to destroy the plasma wave as the amplification focuses and defocuses selected slices of the beam. This problem was solved by seeding the self-modulated instability (SMI) with a short electron bunch [5], a laser pulse [6] or a sharp cut in the bunch profile[4]. This will promote a single mode and suppress other modes, including the strongest competing modes, the hosing modes [7] and produce well-separated micro-bunches.

3.2. Uniform-density plasma cell

The plasma wavelength is $\lambda_{pe} \approx 1.26\,\mathrm{mm}$ meaning that the 10 cm proton bunch will have to be split into ~ 100 micro-bunches in order to be able to drive the wake. Each micro-bunch contributes to the wakefield, and only if the plasma density is uniform will the contribution of each bunch be coherent. Incoherence will cause the electron bunches to arrive at the wrong phase in the plasma oscillation. An increase in the plasma density will shorten the plasma wavelength causing the electron bunch to crest plasma wave it was riding and fall into the defocusing phase of the plasma wave as shown in Fig 1(a). A decrease in the plasma density will increase the plasma wavelength causing the plasma wave to fall further behind the electron bunch meaning the electron bunch to fall into the trough of the plasma wave resulting in a deceleration of the electron beam 1(c). The electron beam must be in the region of length $\lambda_{pe}/4$ between the defocusing and decelerating phases of the plasma wave.

This requirement of the plasma limits the plasma selection to being uniform rubidium vapor, ionised by a co-propagating laser pulse [9, 10]. Rubidium was chosen due to it's low ionization potential and heavy atomic mass. A heavy element is required to minimize the movement of the plasma's nuclei which causes adverse effects on the plasma's behaviour [11, 12]. The Rubiduim vapor is kept in thermodynamic equilibrium at a constant temperature and volume.

3.3. Injection of the witness beam

Due to SMI, the shape of the drive beam changes in the plasma and for the first four meters, the difference between the phase velocity of the wakefield and the proton beam velocity is quite large and this will effect the electron beam in the same manner as having a non uniform plasma, detailed above. To avoid this problem it was suggested that the electrons could be injected into the plasma after SMI had fully developed. The design of the injection method arrived at passing the electron beam through a

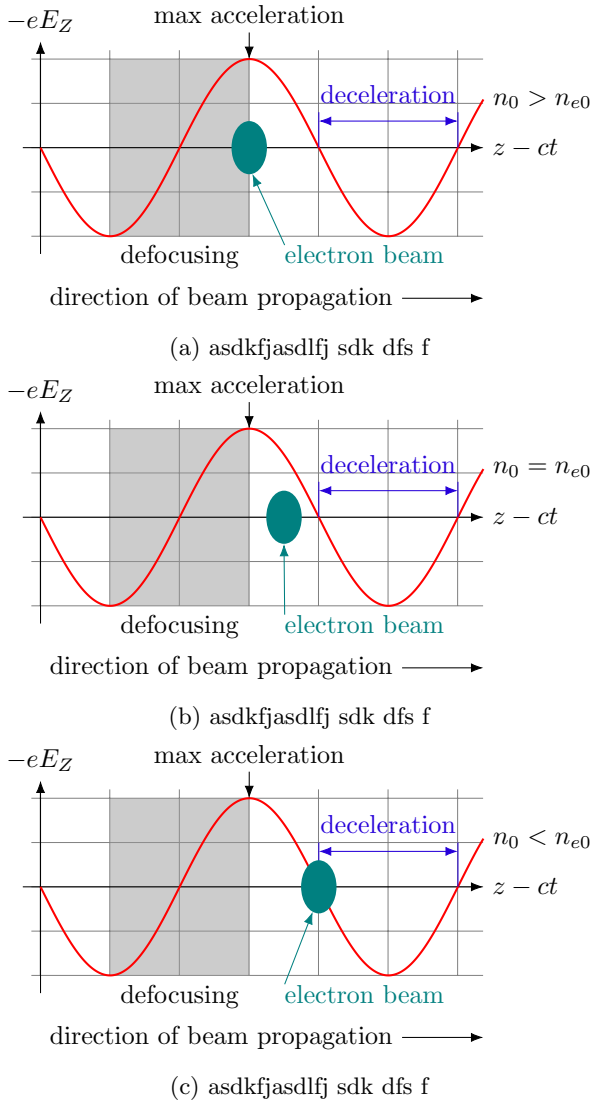

(a) asdkfjasdlfj sdk dfs f

(b) asdkfjasdlfj sdk dfs f

(c) asdkfjasdlfj sdk dfs f

Figure 1: Phasing of the electron bunch for increased density (a) correct density (b) and decreased density (c). [8]

narrow vacuum tube separated from the plasma by a thin foil. Then after $\sim 4\,\mathrm{m}$ the electrons will be directed into the wakefield close close behind the proton driving beam.

3.4. AWAKE

The aim of this experiment is to provide a proof of concept for proton driven plasma wakefield acceleration. An overview of the experiment is as follows:

The SPS will provide the 400 GeV proton driver beam with a bunch length of $\sigma_z = 12\,\mathrm{cm}$ and an intensity of $\sim 3\times10^{11}$ protons/bunch. This will travel down the 750 m long CNGS transfer line and be focused to $\sigma_{x,y} = 200\,\mu\mathrm{m}$ and enter a 10 m long Rubiduim vapor plasma cell with an adjustable density at the 10^{14} to 10^{15} electrons/cm^{-1} scale.

The proton driver will self modulate at the plasma wavelength λ_{pe} after being seeded by a high powered $\approx 4.5\,\mathrm{TW}$ laser pulse that is co-axial and co-propagating with the proton driver beam. This laser also serves the purpose of ionising the Rubidium vapor. These two beams need to be synchronous to within 100 ps and the focal point of the proton beam is required to be $\leq 100\,\mu\mathrm{m}$ and $\leq 15\,\mu\mathrm{rad}$ so they are co-axial for the full length of the plasma cell.

The electron witness beam will be created via photoemission by an illuminating cathode electron source and accelerated by a 2.5 cell RF-gun and a meter long booster at 3 GHz.

4. Project outline

The development of this experiment has been heavily simulation driven. Simulation code developed specifically for the simulation of the plasma to be able to resolve for time scales of ω_p^{-1}, (where ω is the frequency of the plasma wave) and length scales of down to c/ω_p, as existing codes were not tuned to resolve at these scales. Different simulation softwares are tuned to be used for different sections of the AWAKE experiment.

5. Single Particle Dynamics

Equations of motion for charged particles under the effects of accelerator components, such as dipoles and quadrupoles, can be derived through the application of Maxwell's equations []. The solutions to these equations become increasingly complex at higher perturbations so it is usefull to devise a system from which we are ???

Specifying a coorindate system such that the origin follows the ideal path of the particle beam, rather than a coordinate system about an arbitary fixed point we are able to describe the state of a patricle by

$$\begin{pmatrix} x(z) \\ x'(z) \\ y(z) \\ y'(z) \end{pmatrix} = \begin{pmatrix} C_x(z) & S_x(z) & 0 & 0 \\ C'_x(z) & S'_x(z) & 0 & 0 \\ 0 & 0 & C_y(z) & S_y(z) \\ 0 & 0 & C'_y(z) & S'_y(z) \end{pmatrix} \begin{pmatrix} x_0 \\ x'_0 \\ y_0 \\ y'_0 \end{pmatrix} \quad (1)$$

where x and y are deviations form the centre of the beam along their respective axis and x' and y' are the transverse momenta of the particle perpendicular to z, the direction of travel of the beam. Transformations in either the x or y plane are independent, however, it is clear that coupling effects can still be included

6. Emittance

The beam emittance is a qualitative way of describing the quality of the beam, essentially, it is a measure of how parallel the particles of the beam are to each other. It is a conserved quantity in the absence of a z component (i.e. in the direction of the beam) in the magnetic field and when the beam is not being accelerated.

The position of each particle in Cartesian coordinates is not sufficient in describing the state of a beam so each beam particle is represented in six-dimensional phase space with coordinates (x, p_x, y, p_y, z, p_z) where $p_x \approx p_0 x'$ and $p_y \approx p_0 y'$ are the transverse momenta, z is the position along the beam trajectory, p_z is the longitudinal momentum and x' and y' are the trajectory angles to the horizontal and vertical planes. Since the transverse momenta, and therefore x' and y', are generally quite small we can approximate $\sin(x') \approx x'$ and $\sin(y') \approx y'$. We can then project this six-dimensional volume into three independent two-dimensional phase planes, because in this approximation there is no coupling between those degrees of freedom.

The horizontal emittance of the beam is defined by considering the ellipse in the $x' - x$ phase space that contains 95% of all the particles [13]. The area contained by this ellipse divided by π is defined as the emittance in units of π-mm-mrad.

$$\int_{\text{ellipse}} \mathrm{d}x\mathrm{d}x' = \pi\epsilon$$

Fig. 2 shows a beam projected onto a two dimensional phase plane. The emittance can be described by the equation of the ellipse:

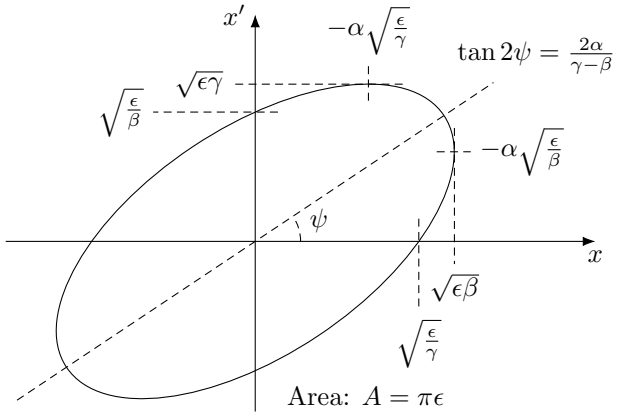

Figure 2: Graphical representation of the relation between the twiss parameters [14]

$$\gamma x^2 + 2\alpha x x' + \beta x'^2 = \epsilon$$

where α, β are γ are ellipse parameters that determine the ellipse's shape and orientation and are related by this equation

$$\beta\gamma - \alpha^2 = 1$$

It follows that the beam matrix is

$$\sigma = \begin{pmatrix} \sigma_{1,1} & \sigma_{1,2} \\ \sigma_{2,1} & \sigma_{2,2} \end{pmatrix} = \begin{pmatrix} \beta\epsilon^2 & -\alpha\epsilon^2 \\ -\alpha\epsilon^2 & \gamma\epsilon^2 \end{pmatrix}$$

such that $\epsilon = \det\sigma$, $\sigma_{1,1}$ is the besm size and $\sigma_{1,2}$ is the orientation in phase space. We can relate the beam matrix after passing through quadrupoles, σ_1, to the original beam matrix, σ_0, as follows

$$\sigma_{1,11} = c^2(k)\sigma_{0,11} + 2c(k)s(k)\sigma_{0,12} + s^2(k)\sigma_{0,22}$$

where we plot the final beam size $\sigma_1, 11$ against the quadrupole strength k. σ_0 is determined from the fit and it's determinant will then give the emittance.

7. The Simulation

The simulation of this experiment was split into three logical parts: the simulation of the beam, the background and camera readout simulation, and the reconstruction of the beam. It is designed such that each part of the code is able to act indepentently.

7.1. The Electron Beam

Given enough computing power and time, the simulation of the beam exiting the plasma cell, passing through two quadrupoles and through a dipole could have been done on BDSIM, a Geant4 toolkit for simulating radiation traveling through an accelerator. This software package takes a particle and updates it's position and velocity each step through the accelerator, applying the affect of forces from all fields within the accelerator. For beams of 1×10^9 electrons, tracking each particle as it travels down the beamline is impractical, therefore a new software was written that simulated the beam as a whole.

7.1.1. BDSIM calibration

BDSIM was used to simulate the firing of 100 000 single electrons down the AWAKE beamline. These electrons had a square energy distribution, from 0–10 TeV and no transverse momentum meaning no emittance. These were used to plot

Since the effect of the dipole on the beam depends on the energy of each individual particle, the evolution of the beam through the dipole cannot be calculated reasonably using beam matrices. So, to simulate the dipole,

7.1.2. Deriving the Beam Size Function

The root mean square of the vertical beam size on the screen can be extracted from the resultant beam matrix **??**.

The beam matrix element $\sigma_{11} = \langle y^2 \rangle = \epsilon\beta$

Multiplying the transport matricies for the quadrupoles and drifts

After generating, a two dimensional histogram representing the number of electrons hitting the screen at each pixel the goal is to simulate the effectiveness of the equipment and translate this number to represent the raw signal that will be read off each pixel.

7.2. Backgrounds

How well the measurement of the emittance is, is most dependant on the magnitude of the multiple sources of backgrounds as well as the reliability of the equipment. The following sources of error were taken into account: the efficiency of the scintillator screen, the acceptance of the camera, the background photon density, the emittance of photoelectrons, the thermal noise, the microchannel plate (MCP) and the readout noise. Each source of noise is added to each pixel independently.

The first two error sources, the scintillator screen and the camera acceptance, both scale the signal. So for each electron that hits the screen, it is expected that an average of 5000 [] photons are to be emitted. The camera acceptance, is the ratio of photons that the camera registers to the number of photons emitted by the scintillator, with a value of 1.5×10^{-5}. After the addition of these two effects, the camera is expected to receive 7.5 % of the original electron signal. The expected value for the number of photons incident on the camera due to the beam electrons is a Poisson random number.

It is assumed that there is a uniform distribution of photons incident on the camera. The density of these electrons is expected to be $1 \times 10^5\ \mathrm{m}^{-2}$ equating to 0.01 background photons per pixel during the 3×10^{-3} the gate is open. This is a discrete value, and so is also a Poisson random number. As discussed later in Section 8 this value is very small in comparison to the signal produced by the beam and will only have an effect if the density of background photons is multiple magnitudes larger than the expected value.

The camera's photomultipliers then convert the photons of light back to an electrical current. This multiplies the incident number of photons by the quantum efficiency of the camera, 0.15 []. The expected number of thermal photoelectrons per pixel per second is expected to be 0.016 at −30 °C with 16 °C cooling water and an ambient room temperature of 16 °C. This value is typically doubles for each 5 °C rise in temperature of the camera.

The microchannel plate amplifies the number of photoelectrons by 1442 amplifying all previously added backgrounds. This was simulated by simply scaling the value of the bin by this value rather than generating a Poisson random number centred about this value.

And finally, before the values of the signal is obtained, a readout noise is added. This backgorund is expected to add 7.2 readout electrons per image pixel for the camera operating at 1 MHz.

7.3. Error Calculations

Poisson statistics were used for the calculation of errors. Once the shape of the incident beam on the screen was calculated the number of electrons incident on each pixel was given an error of the square root of the count. Two methods of error propagation were used depending on the nature of the process involved. The following processes are additive: the background photons, the thermal photoelectrons and the readout noise, whereas the multiplicative processes are: photon generation at the scintilator screen, photoelectron generation in the camera PMTs and the amplification of the electron signal by the MCP.

Basic error propagation techniques were used here. For the additive processes, where the new value of each bin n is the sum between the old bin value n_0 and the value given by the process n_{proc}: $n = n_0 + n_{\mathrm{proc}}$ the propagation of error is given by calculating the hypotenuse of the absolute errors:

$$\delta n = \sqrt{\delta n_0^2 + \delta n_{\mathrm{proc}}^2} \tag{2}$$

where the error of a Poisson random number is the square root of the value.

For the multiplicative processes, i.e. $n = \lambda_{\text{proc}} n_0$ where λ_{proc} is the scaling factor of the process the propagation of the error is given by calculating the hypotenuse of the percentage errors:

$$\delta n = n \sqrt{\left(\frac{\delta n_0}{n_0}\right)^2 + \left(\frac{\delta n_{\text{proc}}}{n_{\text{proc}}}\right)^2} \tag{3}$$

7.4. Binning errors

Initial result

8. Results

8.1. Energy Spread

Initially, the mean energy of the beam and energy spread of the beam were

8.2. Input Emittance

8.3. Background Photons

9. Conclusion

[1] C. O'Luanaigh, "First images of collisions at 13 tev," May 2015.
[2] R. Barate *et al.*, "Search for the standard model Higgs boson at LEP," *Phys. Lett.*, vol. B565, pp. 61–75, 2003.
[3] D. Brandt, H. Burkhardt, M. Lamont, S. Myers, and J. Wenninger, "Accelerator physics at LEP," *Rept. Prog. Phys.*, vol. 63, pp. 939–1000, 2000.
[4] N. Kumar, A. Pukhov, and K. Lotov, "Self-modulation instability of a long proton bunch in plasmas," *Physical review letters*, vol. 104, no. 25, p. 255003, 2010.
[5] K. Lotov, G. Lotova, V. Lotov, A. Upadhyay, T. Tückmantel, A. Pukhov, and A. Caldwell, "Natural noise and external wakefield seeding in a proton-driven plasma accelerator," *Physical Review Special Topics-Accelerators and Beams*, vol. 16, no. 4, p. 041301, 2013.
[6] C. Siemon, V. Khudik, S. A. Yi, A. Pukhov, and G. Shvets, "Laser-seeded modulation instability in a proton driver plasma wakefield accelerator," *Physics of Plasmas (1994-present)*, vol. 20, no. 10, p. 103111, 2013.
[7] J. Vieira, W. Mori, and P. Muggli, "Hosing instability suppression in self-modulated plasma wakefields," *Physical Review Letters*, vol. 112, no. 20, p. 205001, 2014.
[8] H. Wiedemann *et al.*, *Particle accelerator physics*, vol. 314. Springer, 2007.
[9] E. Öz and P. Muggli, "A novel rb vapor plasma source for plasma wakefield accelerators," *Nuclear Instruments and Methods in Physics Research Section A: Accelerators, Spectrometers, Detectors and Associated Equipment*, vol. 740, pp. 197–202, 2014.
[10] E. Öz, F. Batsch, and P. Muggli, "A Novel Laser Ionized Rb Plasma Source for Plasma Wakefield Accelerators," in *Proceedings, 5th International Particle Accelerator Conference (IPAC 2014): Dresden, Germany, June 15-20, 2014*, p. TUPME073, 2014.
[11] J. Vieira, R. A. Fonseca, W. B. Mori, and L. O. Silva, "The ion motion in self-modulated plasma wakefield accelerators," *Phys. Rev. Lett.*, vol. 109, p. 145005, 2012.
[12] J. Vieira, R. A. Fonseca, W. B. Mori, and L. O. Silva, "Ion motion in the wake driven by long particle bunches in plasmas," *Phys. Plasmas*, vol. 21, p. 056705, 2014.
[13] J. Buon, "Beam phase space and emittance," *CERN European Organization for Nuclear Research-Reports-CERN*, pp. 89–89, 1994.
[14] A. Caldwell *et al.*, "Path to AWAKE: Evolution of the concept," *Nucl. Instrum. Meth.*, vol. A829, pp. 3–16, 2016.